ELSEVIER

1 March 1999

OPTICS COMMUNICATIONS

Optics Communications 161 (1999) 13–18

# Profilometry for the measurement of 3-D object shapes based on regularized filters

J. Villa, M. Servin *, L. Castillo

*Centro de Investigaciones en Optica, Apdo. Postal 1-948, Leon, Guanajuato 37000, Mexico*

Received 2 September 1998; revised 22 October 1998; accepted 7 January 1999

**Abstract**

Regularized filters (RFs) are used in profilometry for the measurement of three-dimensional object shapes. A linear grating pattern projected onto an object is phase-modulated by the 3-D shape. Phase information of the pattern is obtained by a demodulation process using RFs based on Bayesian estimation theory with Markov Random Fields (MRFs) as prior models. The technique is fully processed in the space domain and applied in the 2-D case to provide a better separation of the height information from noise. As shown herein, the technique is not so sensitive to the singularities in the pattern image as with common filters used in the spatial synchronous detection. The technique and experimental results of real surface profiles are presented. 

*PACS:* 42.30.−d; 42.30.Rx; 42.30.Tz
*Keywords:* Regularized filters; Profilometry; Markov random fields

## 1. Introduction

The use of projected gratings for the measurement of surface shapes is a well-known technique [1]. This is an easy and efficient way to characterize three-dimensional information because the grating is phase-modulated according to the topography of the object. We can record the 2-D pattern that carries the 3-D information of the object. The remaining task is to retrieve the 3-D information from the pattern by a demodulation process. Several techniques for demodulation have been used: Fourier domain techniques [1–5], phase stepping [6], spatial synchronous detection [7], electronic communication techniques [8,9], and two-frequency grating projection [10]. These techniques require no fringe-order assignment and need no interpolation between fringes, since every pixel in the image may give height information.

A method on the 1-D Fourier domain was proposed by Takeda and Mutoh [1] and Takeda et al. [2]. This method was improved by Li et al. [3] by using a defocused projected grating. The same method was used to get moiré expressions by Suganuma and Yoshizawa [4]. The analysis of Takeda et al. was extended to a 2-D Fourier domain by Lin and Xian [5] to provide a better separation of height information from noise. Tang and Hung [7] proposed the synchronous method using an FIR filter.

Fourier methods need an image size of $2^n$ and a full field pattern to work properly, this is a disadvantage, since in most real situations, this is not possible because of the finite size of the object; furthermore, the most common convolution filters used in the spatial synchronous detection are so sensitive to their parameters, noise, and regions with singularity neighborhoods in the pattern that may require a more robust unwrapping process.

The problem of finding a phase function given the observations (i.e., the grating pattern) may be considered an ill-posed problem, since the task is to recover the 3-D information from a 2-D fringe pattern image. This problem

* Corresponding author. E-mail: mservin@foton.cio.mx

0030-4018/99/$ - see front matter 
PII: S0030-4018(99)00010-3

may be turned into a well-posed one if it is given some prior information about the smoothness of the shape. The Bayesian approach to model cost functionals is used to construct regularized filters (RFs) [11,12]. This kind of filters yield good performance in situations in which convolution filters fail, since they are relatively insensitive to edge effects and may interpolate over regions of missing data with well-defined behavior. The technique may also be used in profilometry and applied in the two-dimensional case to provide a better separation of the height information from noise, when speckle-like structures and discontinuities in the observed grating pattern are present.

## 2. Optical geometry for height measurement

The typical crossed-optical-axes geometry of the projection and recording system for the height measurement is shown in Fig. 1. The optical axes of the projector and the camera cross at point O on an imaginary plane R that serves as a reference from which object height is measured. Ep and Ec denote the projection centers of the projector and the CCD camera, respectively. L is an imaginary plane on which the image of the grating is formed. The distance between Ep and Ec is denoted by $d$, and $l_0$ is the distance between Ec and O. $P$ is the period of the projected grating. The lines of the grating are normal to the plane of the figure.

If the grating is defocusedly projected onto the object [3], the image observed through the CCD camera will have a quasi-sine distribution which can be written as

$$g(x,y) = a(x,y) + b(x,y)\cos\left[2\pi f_0 x + \phi(x,y)\right] \quad (1)$$

$$\phi(x,y) = \phi_0(x,y) + \phi_z(x,y) \quad (2)$$

where $f_0$ is the fundamental frequency of the observed grating image; $a(x,y)$ and $b(x,y)$ are the background and the amplitude modulation, respectively; $\phi_0(x,y)$ is the phase modulation by diverging illumination in $h(x,y) = 0$; and $\phi_z(x,y)$ is the phase shift due to the object's height distribution, thus

$$\phi_z(x,y) = \phi(x,y) - \phi_0(x,y) = 2\pi f_0 \overline{\mathrm{CD}} \quad (3)$$

and the formula to obtain the height distribution is [1]

$$z(x,y) = \frac{l_0 \overline{\mathrm{CD}}}{\overline{\mathrm{CD}} - d} = \frac{l_0 \phi_z(x,y)}{\phi_z(x,y) - 2\pi f_0 d}. \quad (4)$$

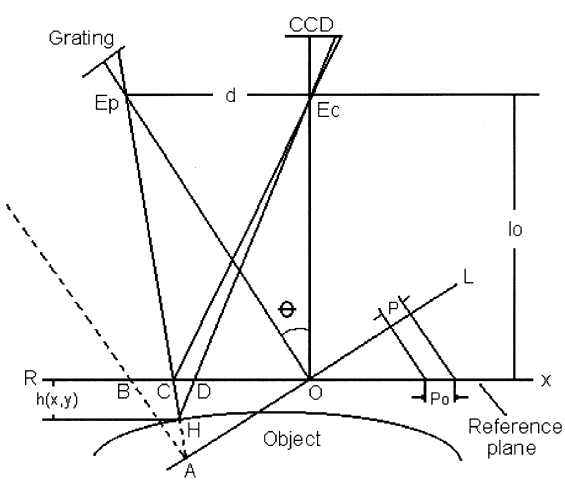


Fig. 1. Optical geometry for height measurement.

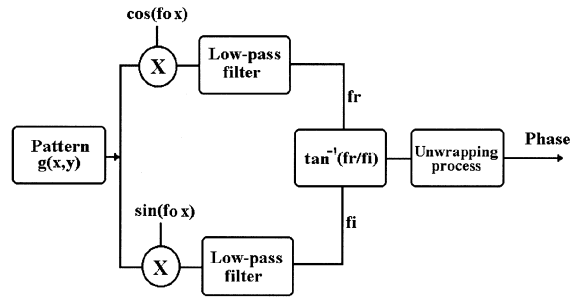


Fig. 2. Typical synchronous demodulation scheme.

## 3. Phase measurement for retrieving the object shape

### 3.1. Spatial synchronous detection

As mentioned above, the fringe pattern may be represented by Eq. (1) where $\phi(x,y)$ has the height information which varies slowly compared with the phase carrier. Using the spatial synchronous detection method, the phase is calculated by [13]

$$\phi(x,y) = \tan^{-1} - \frac{h(x,y) * \left[ g(x,y)\sin(2\pi f_0 x)\right]}{h(x,y) * \left[ g(x,y)\cos(2\pi f_0 x)\right]}$$

$$= \tan^{-1} - \frac{h(x,y) * g_s(x,y)}{h(x,y) * g_c(x,y)} \quad (5)$$

where the asterisk denotes convolution and $h(x,y)$ a low-pass filter which can be a single average window or those FIR filters proposed by Tang and Hung [7]. A schematic diagram of the synchronous demodulation is shown in Fig. 2.

### 3.2. Regularized filters

Filtering is a task that has been widely used in signal processing and pattern analysis to smoothen or to isolate the desired signal from noise. The task may also be considered as an estimation problem in which we are interested in reconstructing a smooth function $f$ at the sites

of a lattice $L$, given the observations $g$ (e.g., the fringe pattern) where the noise $n$ is present

$$g(x) = Hf(x) + n(x), \qquad x \in S. \tag{6}$$

In the model, $H$ is a noninvertible operator that represents some kind of degrading operation and $S$ is a subset of $L$ where the observations are available. This problem is considered ill-posed because the observation process $g$ does not determine the value of $f$ in a unique and stable way. The Bayesian approach to regularize this kind of problem requires prior knowledge of $f$. The estimated signal may be obtained as the minimizer (the maximum a posteriori estimator) of an energy functional of the form [11,12]

$$U(f) = \sum_{x \in S} \Phi_{f,g}(x) + \lambda \sum_{C} U_C(f) \tag{7}$$

The first term on the right side of Eq. (7) is related to the fidelity between the estimated function and the observation; the second term is related to the smoothness of the signal to be estimated (i.e., the prior model). Parameter $\lambda$ depends on the noise model (it may also be seen as a parameter that controls the compromise between the degree of regularization and its closeness to the data).

As Marroquin et al. [11] mentioned, the prior models that satisfy the requirements in the stochastic route to regularize this kind of problems are the Markov Random Fields (MRFs) on finite lattices. MRFs are defined by a set $C$ of potential functions $U_C$ that ranges over the cliques associated with a given neighborhood system. The following are the most important characteristics of MRFs.

(1) The probabilistic dependences between the elements of the field are local. This is important because we need to model surfaces that are only piecewise smooth; in this way, the reconstruction algorithms can be efficiently implemented in parallel hardware.

(2) The class of MRFs is rich for a wide variety of qualitatively different behaviors to be modeled. In particular, if we assume that the noise is Gaussian, we choose $f$ that minimizes the squared error in the first term of the functional (7). When we assume that the $f$ field has to be globally smooth, the potential functions are usually chosen as squares of discrete approximations to partial derivatives which may be the second order (thin-plate) MRF model,

$$\begin{aligned} U[f(x,y)] = &\sum_{(x,y)\in S} [f(x,y) - g(x,y)]^2 \\ &+ \lambda_x \sum_{x \in C_x} [f(x+1,y) - 2f(x,y) \\ &+ f(x-1,y)]^2 \end{aligned} \tag{8}$$

Setting the gradient of Eq. (8) equal to zero, we get a set of equations of the form

$$\begin{aligned} \frac{\partial U}{\partial f(x,y)} = &f(x,y) - g(x,y) + \lambda_x [6f(x,y) \\ &- 4f(x+1,y) - 4f(x-1,y) + f(x+2,y) \\ &+ f(x-2,y)] = 0. \end{aligned} \tag{9}$$

The minimization operation may be considered as a robust low-pass filter in the $x$ direction acting on $g$ that interpolates over sites where information is missing. Taking the Fourier transform for the variable $x$ of Eq. (9), the transfer function of the filter is obtained and expressed as

$$\begin{aligned} H(\omega,y) &= \frac{F(\omega,y)}{G(\omega,y)} \\ &= \frac{1}{1 + \lambda_x [6 + 2\cos(2\omega,y) - 8\cos(\omega,y)]}. \end{aligned} \tag{10}$$

One can obtain the minimizer $f(x,y)$ by performing the steepest descent algorithm,

$$f^{k+1}(x,y) = f^k(x,y) - \mu \frac{\partial U}{\partial f(x,y)}, \tag{11}$$

where $\mu$ is the step size. The filtering operation may be performed in the same way for both $g_s(x,y)$ and $g_c(x,y)$.

In an ideal case without noise, 1-D filtering could be enough to separate the desired signal. However, there are applications in which some speckle-like structures, discontinuities and regions of missing data could cause phase inconsistencies [5]. Therefore, a 2-D filtering is necessary.

To obtain a regularization functional for a low-pass filter in the $y$ direction, we can use a regularization term that corresponds to an MRF in the $y$ direction

$$\begin{aligned} U[f(x,y)] = &\sum_{(x,y)\in S} [f(x,y) - g(x,y)]^2 \\ &+ \lambda_y \sum_{y \in C_y} [f(x,y+1) - 2f(x,y) \\ &+ f(x,y-1)]^2, \end{aligned} \tag{12}$$

which corresponds to the set of equations

$$\begin{aligned} \frac{\partial U}{\partial f(x,y)} = &[f(x,y) - g(x,y)] + \lambda_y [6f(x,y) \\ &- 4f(x,y+1) - 4f(x,y-1) + f(x,y+2) \\ &+ f(x,y-2)] = 0 \end{aligned} \tag{13}$$

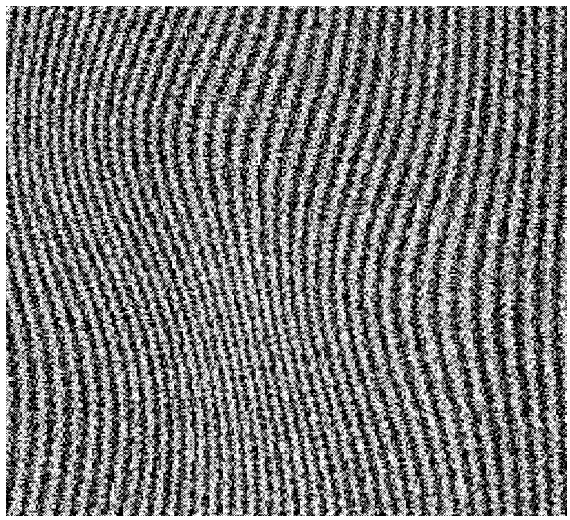

Fig. 3. Simulated fringe pattern with uniformly distributed phase noise ranging from $-\pi/2$ to $\pi/2$.

It should be noted that the filters are applied sequentially over the fringe pattern being processed.

## 4. Noise sensitivity analysis

In this section, the noise sensitivity of RFs and convolution filters is analyzed and compared. The size of the window for the filters used in the direct method was selected according to a rectangular function that may be represented by [13]

$$h(x,y) = \mathrm{rect}\left(\frac{x}{p_0}\right) \tag{14}$$

and its frequency response

$$H(u,y) = \frac{\sin(\pi u p_0)}{\pi u p_0}, \tag{15}$$

where $u$ is the spatial frequency. Eq. (15) means that the frequency responses of window filters have ringing effects for high frequencies which may introduce errors in the calculated phase.

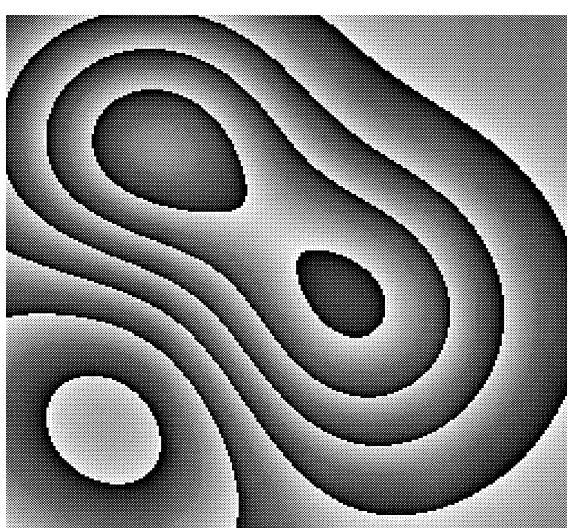

Fig. 4. Modulating phase signal of the fringe pattern shown in Fig. 3.

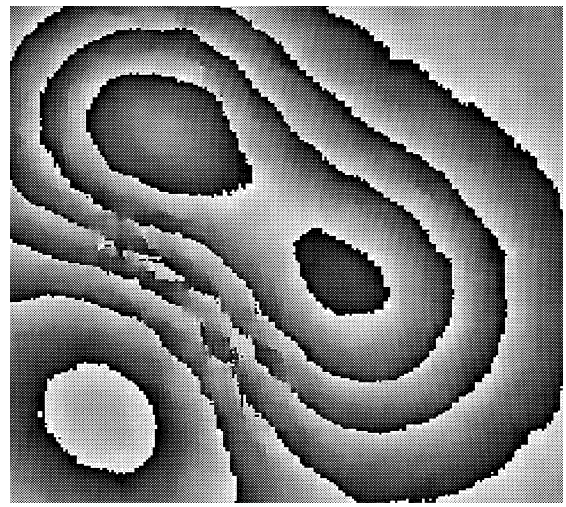

Fig. 5. Phase distribution obtained with the neighborhood average filter.

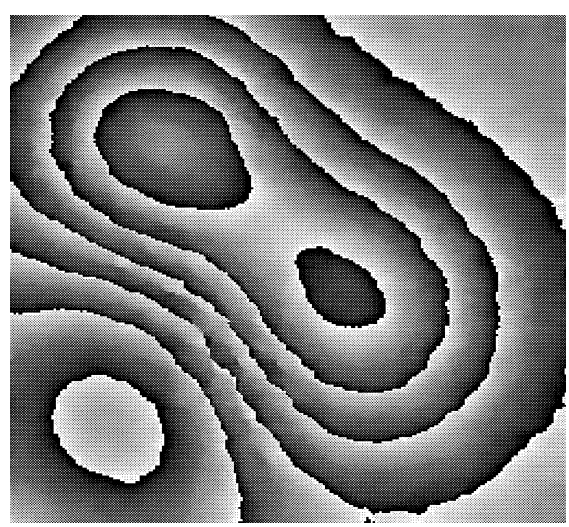

Fig. 6. Phase distribution obtained with the RF.

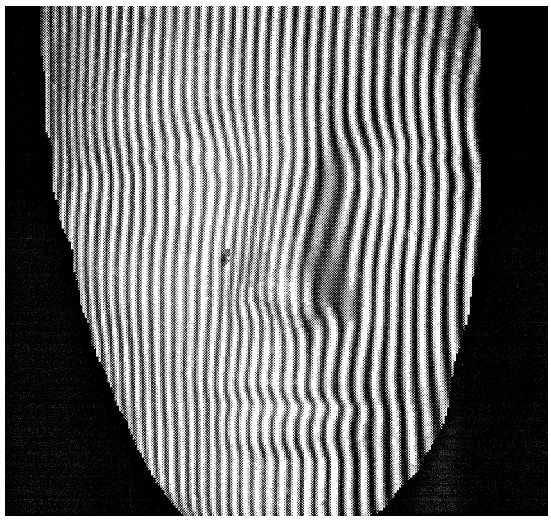

Fig. 7. Deformed grating by an object under test.

We have simulated a noisy wideband fringe pattern with uniformly distributed phase noise ranging from $-\pi/2$ to $\pi/2$. This fringe pattern of $256 \times 256$ pixels with 8-bit gray levels is shown in Fig. 3. The modulating phase signal of Fig. 3 is shown wrapped in gray levels in Fig. 4. The demodulated phase with a neighborhood average filter is shown in Fig. 5. An immediate consequence is the presence of phase inconsistencies in high-frequency regions of the fringe pattern. Fig. 6 shows the phase recovered by using the RF with $\lambda_x = 200$ and $\lambda_y = 150$. The normalized RMS errors of the window filter and the RF were 0.04 and 0.017 rad, respectively.

## 5. Experimental results

A 100 lines/in Ronchi grating was used to be projected by a conventional slide projector. The deformed grating pattern was observed by a CCD video camera (with a 75-mm focal length lens) and stored to be processed into a 133-MHz Pentium computer with a frame memory of $256 \times 256$ pixels (8-bit gray levels). The parameters in the optical arrangement shown in Fig. 1 were $d = 30$ cm and $l_0 = 125$ cm. The period in the pattern image was $p_0 = 5.44$ pixels and the period of the grating projected onto the object was $p = 2.2$ mm.

Two different window filters were used in the spatial synchronous detection to retrieve the height distribution of an object. Fig. 7 shows the fringe pattern image of the grating projected onto an object under test. The calculated size of the window according to Eq. (14) was $M = \text{int}(2\,p_0 + 1) = 11$. An easy sequential unwrapping technique used by Takeda et al. [2] was applied in the experiments. Figs. 8 and 9 show the resulting unwrapped phase obtained using the synchronous detection with an average rectangular window and a Hamming window, respectively. As can be seen, the filters have failed in some shadows and singularities of the pattern. Fig. 10 shows the results obtained using the RF method with $\lambda_x = 200$ and $\lambda_y = 150$.

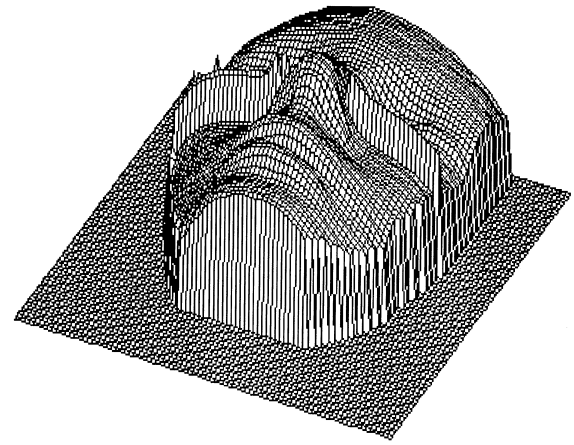

Fig. 9. Height distribution obtained using a Hamming window.

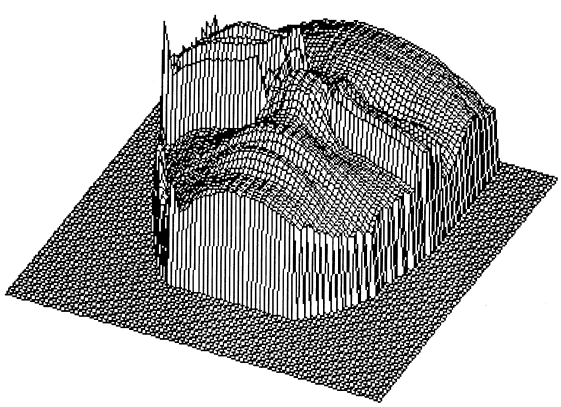

Fig. 8. Height distribution obtained using a rectangular average window.

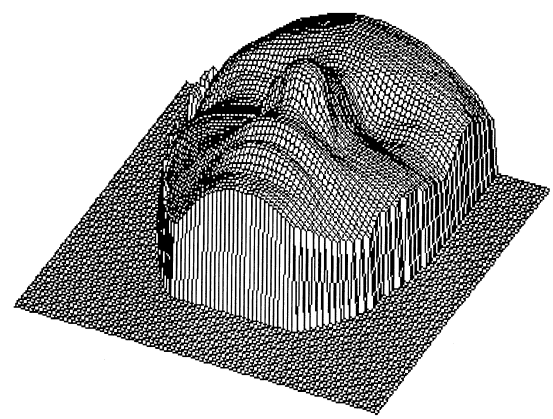

Fig. 10. Height distribution obtained using RFs with $\lambda_x = 200$ and $\lambda_y = 150$.

## 6. Conclusions

The use of RFs for the measurement of 3-D object shapes has been proposed, without the need to cover the whole digitized field and a power of two-image size as normally required by Fourier methods. Furthermore, the advantages of this method with reference to convolution filters used in spatial synchronous detection are its good noise rejection, relatively insensitivity to edge effects and possibility of interpolation over singularity pixels with well-defined behavior. In many cases, the patterns obtained in profilometry have speckle-like structures, discontinuities and data may be lost in the observation process; this is a disadvantage when convolution filters are used. Effectively, the convolution technique is a fast method, but it may require a more robust unwrapping technique which implies a slower process. The main disadvantage using this method is the speed of the minimization process; however, it may be improved using a more efficient algorithm (e.g., the conjugate gradient method).

## Acknowledgements

This work was supported by the Consejo Nacional de Ciencia y Tecnologia (CONACyT), Mexico.

## References

[1] M. Takeda, K. Mutoh, Fourier transform profilometry for the automatic measurement of 3-D object shapes, Appl. Opt. 22 (24) (1983) 3982–3997.
[2] M. Takeda, H. Ina, S. Kobayashi, Fourier-transform method of fringe-pattern analysis for computer-based topography and interferometry, J. Opt. Soc. Am. 72 (1) (1982) 156–160.
[3] J. Li, X. Su, L.-R. Guo, Improved transform profilometry for the automatic measurement of three-dimensional object shapes, Opt. Eng. 29 (12) (1990) 1439–1444.
[4] M. Suganuma, T. Yoshizawa, Three-dimensional shape analysis by use of a projected grating image, Opt. Eng. 30 (10) (1991) 1529–1533.
[5] J.-F. Lin, Y. Xian, Two-dimensional Fourier transform profilometry for the automatic measurement of three-dimensional object shapes, Opt. Eng. 34 (11) (1995) 3297–3302.
[6] H. Su, J. Li, X. Su, Phase algorithms without the influence of carrier frequency, Opt. Eng. 36 (6) (1997) 1799–1805.
[7] S. Tang, Y.Y. Hung, Fast profilometer for the automatic measurement of 3-D object shapes, Appl. Opt. 29 (20) (1990) 3012–3018.
[8] R. Rodriguez-Vera, M. Servin, Phase locked loop profilometry, Opt. Laser Technol. 26 (6) (1994) 393–398.
[9] S. Toyooka, Y. Iwaasa, Automatic profilometry of 3-D diffuse objects by spatial phase detection, Appl. Opt. 25 (10) (1986) 1630–1633.
[10] J. Li, H. Su, X. Su, Two frequency grating used in phase-measuring profilometry, Appl. Opt. 36 (1) (1997) 277–280.
[11] J.L. Marroquin, S. Mitter, T. Poggio, Probabilistic solution of ill-posed problems in computational vision, J. Am. Stat. Assoc. 82 (1987) 76–89.
[12] J.L. Marroquin, Probabilistic solution of inverse problems, Artificial Intelligence Laboratory Rep. TR-860, Massachusetts Institute of Technology, Cambridge, MA, 1985.
[13] A.J. Moore, F. Mendoza, Phase demodulation in the space domain without a fringe carrier, Opt. Lasers Eng. 23 (1995) 319–330.